




## Harnessing superdirectivity in dielectric spherical multilayer antennas

Roman Gaponenko <sup>1</sup>, Alexander Moroz <sup>2</sup>, Ilia L. Rasskazov <sup>3,\*</sup>, Konstantin Ladutenko <sup>1</sup>, Alexey Shcherbakov <sup>1,†</sup> and Pavel Belov <sup>1</sup>

<sup>1</sup>*School of Physics and Engineering, ITMO University, Saint-Petersburg 197101, Russia*

<sup>2</sup>*Wave-scattering.com*

<sup>3</sup>*The Institute of Optics, University of Rochester, Rochester, New York 14627, USA*



(Received 19 March 2021; revised 21 September 2021; accepted 12 October 2021; published 5 November 2021)

Small form-factor, narrow band, and highly directive antennas are of critical importance in a variety of applications spanning wireless communications, remote sensing, Raman spectroscopy, and single photon emission enhancement. Surprisingly, we show that the classical directivity limit can be appreciably surpassed for electrically small multilayer spherical antennas excited by a point electric dipole even if limiting ourselves to purely dielectric materials. Experimentally feasible designs of superdirective antennas are established by using a stochastic optimization algorithm combined with a rigorous analytic solution.

DOI: [10.1103/PhysRevB.104.195406](https://doi.org/10.1103/PhysRevB.104.195406)

### I. INTRODUCTION

Physical limitations on antennas are critical when designing efficient devices. The limitations have been the subject of research since the early age of antenna science [1–3]. There is a trade-off between gain,  $G$ , which defines the spatial narrowness of radiation patterns, and the quality factor,  $Q$ , which characterizes the ratio of the stored energy to emitted power [4].  $Q$  is known to be inversely proportional to the bandwidth when  $Q \gg 1$  [4]. Gain is related to directivity,  $\mathcal{D}$ , through  $G = e_r \mathcal{D}$ , where  $e_r$  is the radiation efficiency of the antenna, taking into account antenna losses (it does not include polarization or impedance mismatch losses). In our paper, we consider purely dielectric antennas. Given that such antennas are lossless ( $e_r = 1$ ), we use only the term *directivity* in what follows without any loss of generality.

The Harrington-Chu limit [2,5] puts an upper bound on the directivity as  $\mathcal{D}_{\text{lim}} = (kR)^2 + 2kR$ , where  $R$  is the radius of the sphere circumscribing an antenna and  $k$  is the free-space wave number. Kildal *et al.* [6,7] improved the formula for directivity limit in the case of small-size antennas to  $\mathcal{D}_{\text{lim}} = (kR)^2 + 3$ . The above expressions for  $\mathcal{D}_{\text{lim}}$  concern the so-called *normal* gain [5] and rely on the hypothesis which postulates a *linear* relationship between the antenna size and the number of spherical harmonic modes,  $kR = \ell$  [5] (see also the field degrees of freedom [8]), that can be efficiently excited by the antenna. The relation of the power radiated by the partial modes to the stored energy yields estimates on  $Q$  and  $\mathcal{D}$  [4,9,10]. However, the directivity is generally known to exceed these limits [1,11]. The antennas with  $\mathcal{D} > \mathcal{D}_{\text{lim}}$  are referred to as *superdirective*.

Recent publications [12–17] show continuing interest in overcoming the physical limitations on antenna design. Most

of them are related to emerging applications and to advances in computer-based approaches to antenna optimization [18] as well as to numerical stability of theoretical treatments [19]. Since the superdirectivity of small antennas originates from their resonant behavior, it is accompanied by an ultranarrow-band response, which limits their applications. Nonetheless, the internet of things and wireless power transfer can benefit from such antennas in the radio frequency band [20]. In the optical band, high-index dielectric and plasmonic nanoparticles were used to enhance the direction-selective absorption and emission of nanoantennas [21]. A convex optimization based on the method of moments developed in Ref. [22] was used to determine optimal surface currents, which allowed both maximum gain and superdirective field patterns [23,24] to be achieved. Although the proposed method is very general, it is unclear how to implement the optimal currents in antenna devices. Here, on using rigorous analytic treatment, we consider a spherical multilayer antenna with a dipole source excitation to demonstrate that particular superdirective designs with operation limits comparable to optimal current configurations [23] are possible even in a relatively simple geometry of small *lossless* dielectric resonant antennas.

### II. THEORY

We consider a lossless dielectric nonmagnetic concentric spherical multilayer antenna excited by an electric point dipole source,  $\mathbf{p}$ , located on the  $z$  axis. Because a dipole emits predominantly in a perpendicular direction to its axis, the far-field radiation of a radially oriented dipole (i.e., parallel to the  $z$  axis) is much more difficult to tailor by a nearby spherical antenna than for the tangential dipole orientation (i.e., perpendicular to the  $z$  axis). For instance, for a radially oriented dipole outside the antenna, the far-field radiation part largely escapes to infinity without ever interacting with the antenna. Out of two possible orthogonal dipole orientations, we thus focus on the *tangential* dipole orientation (see

\*Corresponding author: irasskaz@ur.rochester.edu

†Corresponding author: alexey.shcherbakov@metalab.ifmo.ru

Supplemental Material Sec. I [25]). The center of coordinates is at the sphere's origin. We denote the dipole position,  $r_d$ ; radii of layers,  $R_n$  (where  $n = 1, \dots, N$ ); homogeneous isotropic concentric domains,  $\Omega_n$ ; refractive indices of spherical layer domains,  $\eta_n \geq 1$ ; refractive index of a surrounding medium,  $\eta_{N+1} = 1$  (in the domain  $\Omega_{N+1}$ ). We consider non-magnetic materials with the permeability of a vacuum. Dipole locations both inside and outside the spherical layers are allowed.

Maxwell's equations in each homogeneous layer can be solved via the vector spherical wave expansion of the electric field ([26], Eq. (8)),

$$\mathbf{E}_\gamma(n, \mathbf{r}) = \sum_L [A_{\gamma L}(n) \mathbf{J}_{\gamma L}(k_n, \mathbf{r}) + B_{\gamma L}(n) \mathbf{H}_{\gamma L}(k_n, \mathbf{r})], \quad (1)$$

where  $\mathbf{J}_{\gamma L}$  and  $\mathbf{H}_{\gamma L}$  are varieties of the vector multipoles  $\mathbf{F}_{\gamma L}$  (see Eq. (S1) in the Supplemental Material [25]) which correspond to different linear combinations,  $f_{\gamma \ell}$ , of the spherical Bessel function in a given  $n$ th shell [26]. Subscript  $\gamma$  denotes the polarization:  $\gamma = M$  for magnetic or transverse electric (TE) polarization,  $\gamma = E$  for electric or transverse magnetic (TM) polarization. The vector multipoles  $\mathbf{F}_{ML}$  and  $\mathbf{F}_{EL}$  reduce to  $\mathcal{M}_L$  and  $\mathcal{N}_L$  in the Stratton's notations [27,28] provided that  $f_{\gamma \ell}$  reduces to one of  $j_\ell$  or  $h_\ell^{(1)}$ . The index  $L = (\ell, m)$  incorporates the orbital and magnetic quantum numbers.

The continuity of tangential field components determines the interface conditions allowing us to relate the expansion coefficients  $A_{\gamma L}$  and  $B_{\gamma L}$  in adjacent neighboring regions  $\Omega_n$  and  $\Omega_{n+1}$  via  $2 \times 2$  lowering  $T_{\gamma L}^-$  or raising  $T_{\gamma L}^+$  transfer matrices [26]:

$$\begin{pmatrix} A_{\gamma L}(n+1) \\ B_{\gamma L}(n+1) \end{pmatrix} = T_{\gamma L}^+(n) \begin{pmatrix} A_{\gamma L}(n) \\ B_{\gamma L}(n) \end{pmatrix}, \quad (2)$$

$$\begin{pmatrix} A_{\gamma L}(n) \\ B_{\gamma L}(n) \end{pmatrix} = T_{\gamma L}^-(n) \begin{pmatrix} A_{\gamma L}(n+1) \\ B_{\gamma L}(n+1) \end{pmatrix}. \quad (3)$$

The transfer matrix method of Ref. [26] enables one to calculate the emission of the dipole located either inside or in the vicinity of an arbitrary multilayered sphere. Two boundary conditions are required to unambiguously fix the solution. The so-called *regularity* boundary condition guarantees that the fields is not singular at the sphere core layer. Similarly to the case of Mie scattering from homogeneous spheres, this requires that only  $f_{\gamma \ell} \sim j_\ell$  are allowed in the core layer for  $r < r_d$ . Unlike the case of Mie scattering, the other boundary condition depends on the position of the radiating dipole. For the dipole outside the multilayer sphere, the incoming dipole wave multipole coefficients  $A_{\gamma L}(N+1)$  have to be the coefficients  $\alpha_{\gamma L}^d$  of the electric field of a radiating dipole source located at a position  $\mathbf{r}_d$  of a homogeneous space [29] (cf. Eq. (S10) in the Supplemental Material [25]). For the dipole inside the multilayer sphere, there is no incoming wave arriving from the outside, hence  $A_{\gamma L}(N+1) \equiv 0$ . However, in the layer where the radiating dipole is located, the field expansion becomes [26]

$$\mathbf{E}(\mathbf{r}) = \begin{cases} \sum_{\gamma L} [(A_{\gamma L} + \alpha_{\gamma L}^d) \mathbf{J}_{\gamma L} + B_{\gamma L} \mathbf{H}_{\gamma L}], & r < r_d \\ \sum_{\gamma L} [A_{\gamma L} \mathbf{J}_{\gamma L} + (B_{\gamma L} + \alpha_{\gamma L}^d) \mathbf{H}_{\gamma L}], & r > r_d, \end{cases} \quad (4)$$

with the amplitudes having a *discontinuity* at  $r = r_d$ , because such is the dipole field (cf. Eqs. (S7)–(S10) in the Supplemental

Material [25]). The quantities of crucial interest are the amplitudes  $B_{\gamma L}(N+1)$  for  $r > r_d$ , which determine the radiating field escaping to infinity through the far-field amplitude matrix  $\mathbf{F}(\theta, \varphi)$  (Eq. (S25) in the Supplemental Material [25]). What is very convenient in the case of a multilayered sphere is that the  $B_{\gamma L}(N+1)$ 's can be represented in terms of *m-independent* linear combinations of the dipole field expansion coefficients  $\alpha_{\gamma L}^d$  and  $\alpha_{\gamma L}^d$ . The final solutions for  $B_{\gamma L}(N+1)$  coefficients are strongly dependent on the position of the dipole source  $r_d$ . Four separate cases can be distinguished ([26], Eqs. (60), (63), (65), (66)):

(a) For a dipole in a generic sphere shell different from the core and ambient:

$$B_{\gamma L}(N+1) = \frac{\mathcal{T}_{11;\gamma \ell} \alpha_{\gamma L}^d + \mathcal{T}_{21;\gamma \ell} \alpha_{\gamma L}^d}{\mathcal{M}_{22;\gamma \ell} \mathcal{T}_{11;\gamma \ell} - \mathcal{M}_{12;\gamma \ell} \mathcal{T}_{21;\gamma \ell}}.$$

(b) For a dipole in the sphere core:

$$B_{\gamma L}(N+1) = \alpha_{\gamma L}^d / \mathcal{M}_{22;\gamma \ell}(1).$$

(c) For a dipole outside the sphere with  $r < r_d$ :

$$B_{\gamma L}(N+1) = [\mathcal{T}_{21;\gamma \ell}(N+1) / \mathcal{T}_{11;\gamma \ell}(N+1)] \alpha_{\gamma L}^d.$$

(d) For a dipole outside the sphere with  $r > r_d$ ,

$$B_{\gamma L}(N+1) = \alpha_{\gamma L}^d + [\mathcal{T}_{21;\gamma \ell}(N+1) / \mathcal{T}_{11;\gamma \ell}(N+1)] \alpha_{\gamma L}^d,$$

where  $\mathcal{T}_{\gamma L}(n) = \prod_{x=1}^{n-1} T_{\gamma L}^+(x)$  and  $\mathcal{M}_{\gamma L}(n) = \prod_{x=n}^N T_{\gamma L}^-(x)$  are the ordered products of transfer matrices introduced formally by Eqs. (2) and (3).

Once the amplitudes  $B_{\gamma L}(N+1)$  are known for  $r > r_d$ , the directivity in the direction specified by spherical angles  $(\theta_0, \varphi_0)$  is determined by the formula

$$\mathcal{D}(\theta_0, \varphi_0) = \frac{4\pi r^2 |\mathbf{E}(\mathbf{r})|^2}{r^2 \oint |\mathbf{E}(\mathbf{r})|^2 d\Omega}, \quad (5)$$

where  $|\mathbf{E}(\mathbf{r})|^2$  and  $\oint |\mathbf{E}(\mathbf{r})|^2 d\Omega$  can be expressed via coefficients  $B_{\gamma L}(N+1)$  (see Supplemental Material Sec. I [25]). Therefore, the directivity  $\mathcal{D}(\theta_0, \varphi_0)$  depends on the geometrical and physical parameters of the problem  $R_n, \eta_n, r_d$ , the dipole polarization through the matrix elements of  $\mathcal{T}_{\gamma L}, \mathcal{M}_{\gamma L}$  and dipole amplitudes  $\alpha_{\gamma L}^d$  and  $\alpha_{\gamma L}^d$ .

### III. RESULTS AND DISCUSSION

The best possible theoretical directivity is given by the  $\delta(\theta, \varphi)$  function [30], where physical realization is a plane wave. In the case of the  $\delta$ -function directivity, the expansion coefficients for the fields outside a sphere for  $r > r_d$  have to be

$$B_{\gamma \ell 1}(N+1) \sim i^\ell \sqrt{\frac{2\ell+1}{4\pi}} \quad (6)$$

(cf. plane-wave expansion in Eq. (4.37) of Ref. [28]). Here  $i$  denotes the imaginary unit. The feasibility of this target, which imposes constraints on the geometry and material properties, is examined in Supplemental Material Sec. I [25]. It is shown there that the target can, in principle, be met only for the *tangential* dipole orientation. The coefficients Eq. (6) lead to the Harrington directivity limit  $\mathcal{D}_{\text{lim}} = \ell_{\text{max}}(\ell_{\text{max}} + 2)$  [31] [cf. Eq. (S32)], where  $\ell_{\text{max}}$  is a cutoff on the summation over  $\ell$ .

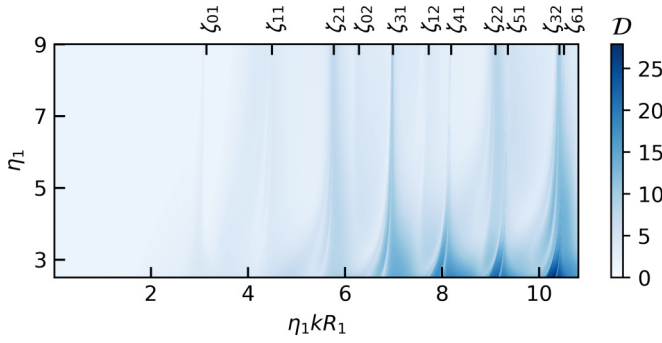


FIG. 1. Optimized directivity  $\mathcal{D}$  of a homogeneous spherical antenna excited by a point electric dipole source at its optimized position as a function of the size parameter  $\eta_1 k R_1$  and refractive index  $\eta_1$ .

Result Eq. (6), which can be seen as a generalization of the results of Ref. [30] for cylindrical geometry in two-dimensional space, is not bounded to a particular geometry and provides a recipe for an ultimate superdirective antenna design in three-dimensional space, useful for a range of applications.

### A. Homogeneous sphere

A special case of a homogeneous spherical antenna represents an example worth careful examination. Figure 1 shows optimized directivity as a function of the sphere's refractive index,  $\eta_1$ , and its size parameter,  $\eta_1 k R_1$ . For each pair of  $\{\eta_1; \eta_1 k R_1\}$ , a dipole position,  $r_d$ , has been optimized to get maximum  $\mathcal{D}$  [see Figs. 2(b) and 2(d)]. Rapid variations in directivity in Fig. 1 are associated with excitation of  $\text{TE}_{(\ell+1)ms}$  and  $\text{TM}_{\ell ms}$  resonance modes in the dielectric sphere according to an approximate condition [32–35],

$$j_\ell(\zeta_{\ell s}) \simeq 0, \quad (7)$$

where  $\zeta_{\ell s} = \eta_1 k R_1$  is the  $s$ th zero of the  $\ell$ th order spherical Bessel functions of the first kind,  $j_\ell$ ;  $\eta_1$  and  $R_1$  are refractive index and radius of a homogeneous spherical dielectric resonator. Table I shows values of  $\zeta_{\ell s}$  for small  $s$  and  $\ell$ . These resonances exhibit themselves by the leakage of trapped electromagnetic field out of high refractive index dielectric scatterer into the environment, leading to resonances of scattered field (interaction between the polarization energy stored in the dielectric and the energy stored in the magnetic field [36]).

Figure 2 shows the dependence of optimized directivity on the refractive index,  $\eta_{\max}$  for  $kR_N \leq 0.314$  and 2.513. According to our numerical results, the maximum directivity for a homogeneous sphere is achieved at  $\zeta_{3s}$  resonances. In general,  $\zeta_{\ell s}$  resonances mainly occur due to the simultaneous excitation of  $\text{TE}_{(\ell+1)ms}$  and  $\text{TM}_{\ell ms}$  modes [34], which is shown in the harmonic expansion plots in Fig. 3. The accurate resonance conditions for these modes are different and the maximum directivity is achieved if all excited modes overlap with optimally tuned amplitudes and phases. The higher the order of overlapping modes, the harder their excitation, since the homogeneous sphere does not have additional degrees of freedom that would allow for simultaneous resonant tuning of

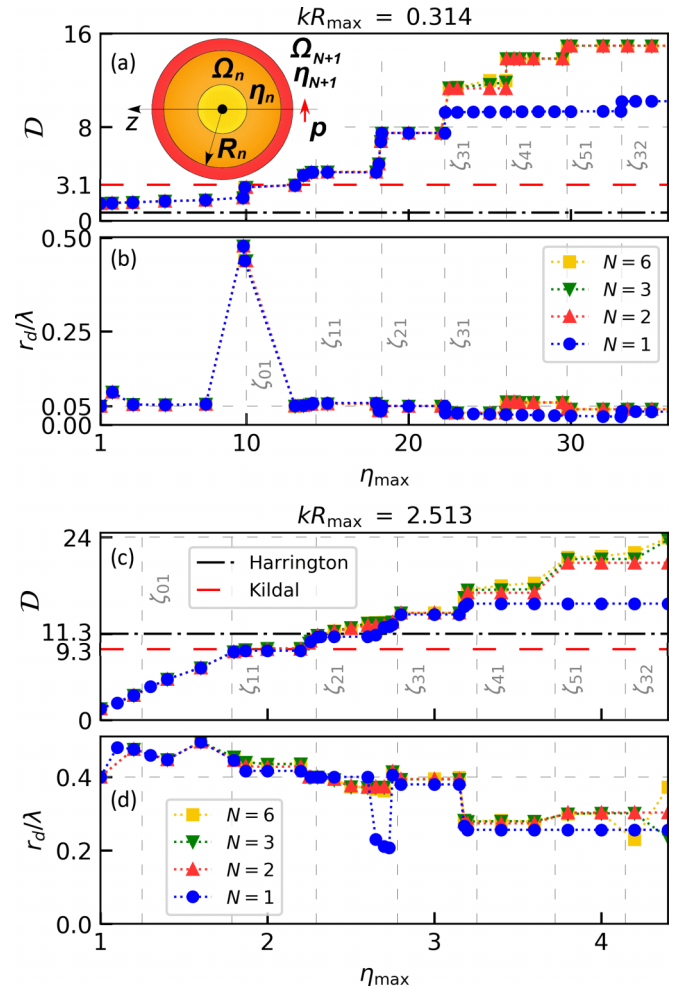


FIG. 2. Maximum achievable directivity and optimum dipole position as a function of the upper bound,  $\eta_{\max}$ , on refractive index for antennas with a different number of layers  $N$ . Sketch of the problem under study is shown in inset in (a). The Harrington and Kildal limits,  $\mathcal{D}_{\text{lim}}$ , are shown in (a) and (c) with black dash-dotted and red dashed lines, respectively.

multiple modes. This is why the value of optimized directivity does not increase for  $\zeta_{\ell s}$  resonances with  $\ell > 3$ .

The position of the exciting electric dipole also affects the order,  $\ell$ , of harmonics excited in the antenna, see Fig. 3. If the dipole source is located at the center of a sphere, only

TABLE I. Zeros  $\zeta_{\ell s}$  of the spherical Bessel function of the first kind  $j_\ell(\zeta_{\ell s}) = 0$ . The subscript  $s$  denotes the ordinal number of the zero of the  $\ell$ th order spherical Bessel function.

	$s = 1$	$s = 2$	$s = 3$
$\ell = 0$	3.14159	6.28319	9.42478
$\ell = 1$	4.49341	7.72525	10.9041
$\ell = 2$	5.76346	9.09501	12.3229
$\ell = 3$	6.98793	10.4171	13.698
$\ell = 4$	8.18256	11.7049	15.0397
$\ell = 5$	9.35581	12.9665	16.3547
$\ell = 6$	10.5128	14.2074	17.648

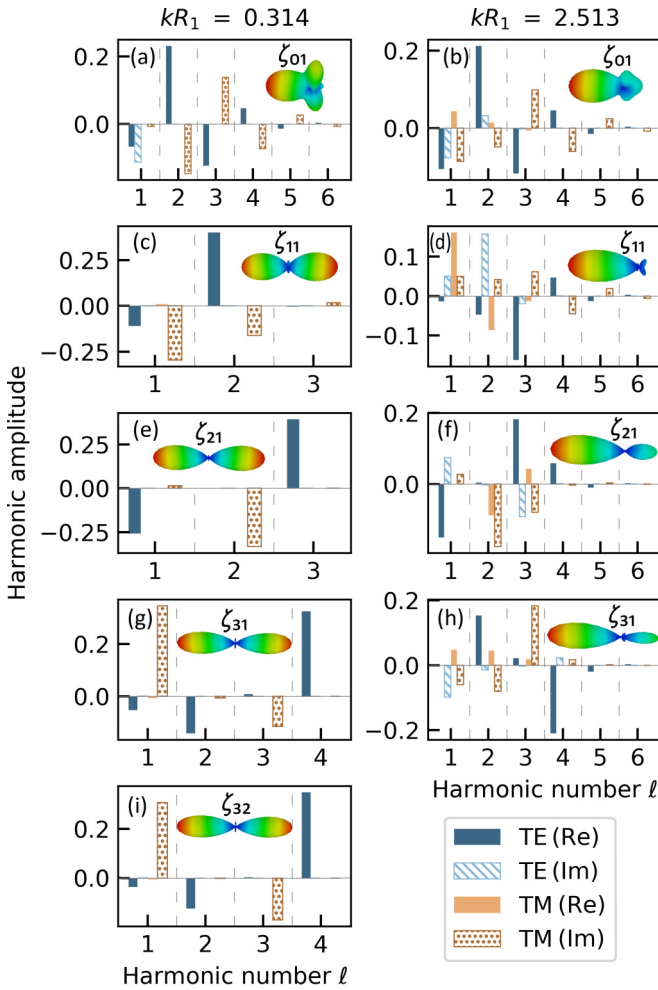


FIG. 3. Normalized harmonic amplitudes at points corresponding to the directivity jumps in Fig. 2 for homogeneous spheres with  $kR_N = 0.314$  and  $kR_N = 2.513$ . The amplitudes are normalized to the sum of the absolute values of the amplitudes for all excited harmonics. Each subplot depicts the corresponding resonance conditions and shows the resulting far-field diagram calculated via full-wave numerical solver CST Studio Suite 2019 [46]. Directivity extracted from far-field diagrams agrees with our theoretical predictions up to 1% accuracy.

$\ell = 1$  is prominent, whereas higher harmonics are induced if the dipole is moved away from the center of the sphere. For example, only  $\ell = 1$  and  $\ell = 2$  harmonics are pronounced for the dipole at position  $r_d = 0.05\lambda$ , while  $\ell = 1, \dots, 6$  are prominent for  $r_d = 0.4\lambda$ , see Figs. 2(b) and 3. We notice that  $\zeta_{01}$  resonance is unique, since in this case the electric dipole source excites only the TE<sub>101</sub> mode (magnetic dipole mode) of the sphere. In order to achieve the highest directivity in the forward direction, electric dipole source and excited magnetic dipole mode must have  $\pi$  phase difference with an optimal dipole position  $r_d \rightarrow \lambda/2$ , see Fig. 2(b) and Ref. [34]. Figure 2(a) makes it clear that a single point electric dipole is not enough to excite resonances  $\zeta_{\ell s}$  of homogeneous sphere with  $\ell > 3$ .

Finally, for electrically small antennas with  $kR_1 \rightarrow 0$ , we observe superdirective behavior at  $\zeta_{3s}$  resonances. With increasing  $s$ , the directivity of the antenna continues to in-

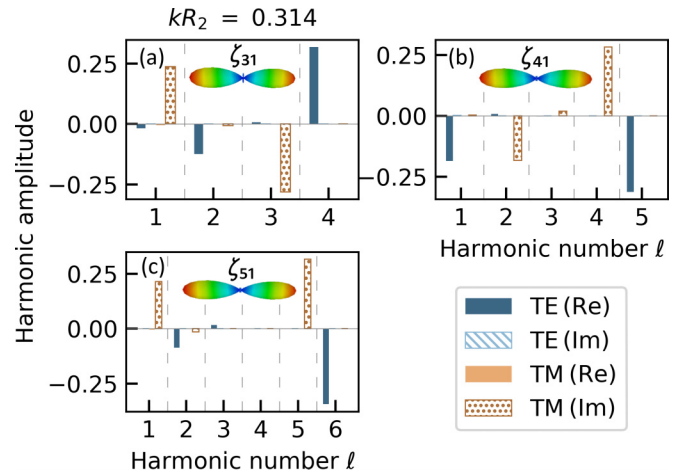


FIG. 4. Same as in Fig. 3, but for two-layer (core-shell) sphere with  $kR_N = 0.314$ .

crease slightly:  $\mathcal{D} > 11.2$  for the resonances with  $s > 14$  (see Table S1 in the Supplemental Material [25]), while the optimal dipole position moves slightly toward the surface of a sphere.

## B. Multilayer sphere

In what follows, we shall use Eq. (5) for direct evaluation of the directivity in the optimization problem for determining maximum directivity  $\mathcal{D}(\theta_0, \varphi_0)$  for a given number of layers  $N$ . We have optimized directivity using the following constraints:

(1) Setting the value of the maximum allowable refractive index  $\eta_{\max}$  of any layer of a sphere and setting the value of  $kR_{\max}$  (see Fig. 2). The refractive indices of layers,  $\eta_n$ , and their sizes,  $R_n$ , are continuously varied within  $1 \leq \eta_n \leq \eta_{\max}$  and  $0 < R_n \leq R_{\max}$  ranges.

(2) Setting the maximum allowable sphere size parameter  $kR_{\max}$  for two different constraints on the refractive indices of layers:

(a) Setting the value of the maximum allowable refractive index  $\eta_{\max}$  and allowing the refractive indices of layers to be continuously varied in  $1 \leq \eta_n \leq \eta_{\max}$  range [see Fig. 5(a)].

(b) Setting the discrete set of allowable refractive indices  $\eta_n \in \{\eta^{(1)}, \eta^{(2)}, \dots\}$ , where  $1 \leq \eta^{(\cdot)} \leq \eta_{\max}$  [see Fig. 5(b)].

The latter strategy is the closest to possible practical implementations, since the set of materials available for fabrication is essentially limited (e.g., high-index ceramics in the radio-frequency band [37] or high-index dielectrics in the optical band [38]), and it is instructive to compare optimization results in these two cases. In any optimization strategy, the position of the dipole,  $r_d$ , is not limited.

Since the convexity of Eq. (5) with respect to the optimization parameters is difficult to establish or check, we used a stochastic JADE algorithm [39] to maximize the directivity. This algorithm is an improved version of the differential evolution, which is effective for global optimization of functions with a large number of local peaks [39,40] and, in particular, for problems associated with electromagnetic scattering



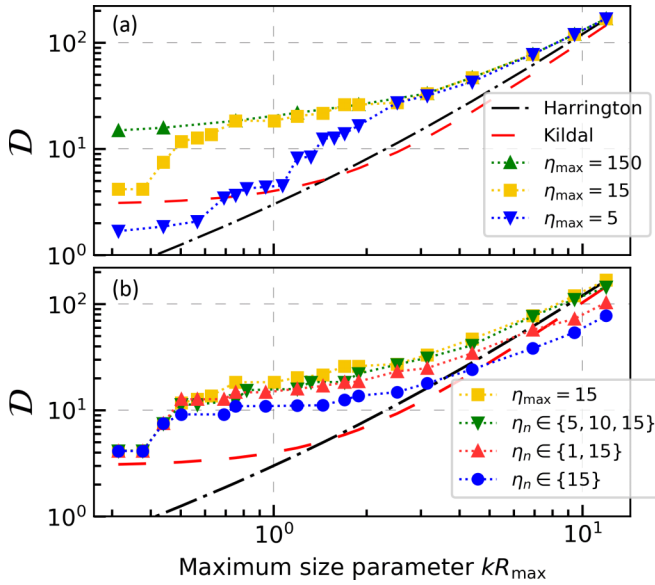


FIG. 5. Dependence of the optimized directivity on the maximum size parameter  $kR_{\max}$  for a spherical three-layer antenna with a different limitation on a refractive index: (a) continuously varying, (b) discrete set.

[41]. For a convergence of the JADE optimization algorithm, one should select appropriate parameters (population size, number of generations, crossover probability, etc.), which strongly depend on the  $Q$  factor of the excited resonances: the higher the  $Q$  factor, the larger value of these parameters is required. Moreover, a numerical implementation of the theoretical treatment presented above requires an accurate truncation of infinite sums to a limited number of terms. As discussed for spherical near-field antenna measurements [42], the recommended number is  $\ell_{\max} = kR_{\max} + x_1$ , where  $kR_{\max}$  is an integer closest to the wave number  $k$  times the radius  $R_{\max} = \max\{r_d; R_N\}$ , and  $x_1$  is an integer which depends on the position of the source and desired accuracy, wherein  $x_1 = 10$  is sufficient for most practical cases [43]. Nonetheless, the relation linking the size parameter with  $\ell_{\max}$  is still questionable for electrically small resonant antennas.

In the lossless case, there is a limit on the directivity for electrically small antennas which depends on the number of layers. Multilayer scatterers can provide higher directivity as shown in Fig. 2 and have more complex resonance conditions, which can be derived from expression Eq. (5). The small multilayer sphere with  $\eta_{\max}kR_N < \zeta_{31}$  usually converges to a homogeneous case. For  $\eta_{\max}kR_N \geq \zeta_{31}$ , directivity optimization results are different, since the additional internal layers can provide more efficient control over the field distribution and over the interference between different multipoles without changing the external size of the antenna. The stored energy of the lower order modes is concentrated closer to the center. Therefore these modes are more sensitive to changes in the internal structure of the sphere and the use of a multilayer structure of a sphere makes it possible to efficiently excite higher-order resonances. Harmonic expansions for several resonances of the two-layer sphere are shown in Fig. 4 (see Supplemental Material Sec. IV [25] for respective data). In the parameter region defined by  $\eta_{\max}kR_N > \zeta_{51}$ ,

it becomes difficult to obtain the global maximum numerically using stochastic optimization procedure for multilayer spheres due to a large number of narrow directivity peaks originating from an interplay between high- $Q$  ( $>10^{10}$ ) TE and TM resonances. In this case, stochastic optimization (i) is computationally expensive, (ii) not necessarily converges to a global maximum, and (iii) requires a large number of initial populations and generations. There are various physical reasons which limit a practically achievable  $Q$  factor of antennas: surface roughness [44,45], material imperfections, the presence of other objects in the immediate vicinity of the antenna, temperature of the environment, and challenging fabrication.

Figure 5 demonstrates the dependence of the optimized directivity  $D$  on the antenna size parameter  $0.3 \leq kR_N \leq 12$  for different limitations on the refractive index of a sphere  $\eta_{\max}$  (taking into account high-index ceramics in the microwave band). Directivity behaves as a step function where the peaks correspond to the interference of the electric dipole with the various induced multipoles of the sphere (either magnetic or electric). Figure 5(a) shows that the use of dielectric materials with  $\eta_{\max} = 15$  allows us to reach the theoretically predicted gain limit for electrically small copper antennas at 1GHz (cf. curve with  $10^{-2}\Omega/\square$  surface resistivity in Fig. 1 of Ref. [23]). Higher refractive index,  $\eta_{\max}$ , or higher applied frequency, in principle, allow us to overcome this limit, which makes high-index ceramics even more attractive. Also, the optimal directivity is almost independent on the formulation of the optimization problem for sufficiently large sets of available refractive indices as demonstrated in Fig. 5(b).  $D$  depends not only on the number of terms in a set but also on the available refractive indices.

An example of optimization for a homogeneous sphere is presented in Supplemental Material Sec. II [25]. Several optimized designs of homogeneous and multilayer spherical superdirective antennas are presented in Supplemental Material Sec. III [25]. The resulting designs for  $kR_N \rightarrow 0$  are generally forward-backward (as a result of constructive interference of the  $TE_{(\ell+1)ms}$  and  $TM_{\ell ms}$  modes in forward and backward directions), while as  $kR_N$  increases, the *forward* direction becomes dominant due to the interference between different modes (see Fig. 2). Occasionally, more complex shapes can be obtained, because optimization is performed in the specified direction  $\theta = 0^\circ$  and does not control the field distribution in other directions.

#### IV. CONCLUSION

Knowing an ideal upper limit on the antenna directivity does not answer the question if the limit can be physically realized. The knowledge of an ideal current configuration on a spherical surface is not of much help if there is no practical way of realizing it. It may well turn out that exotic, i.e., not achievable in practice, material properties will be required to produce ideal current configurations. For a cylindrical antenna driven by a line source, saturating the directivity bounds for a given number  $N$  of layers was already a tedious and difficult task requiring excessive optimization effort and a juxtaposition of positive and negative (i.e., metallic) material regions [30].

Our contribution can be seen in providing explicit engineering recipes for experimentally feasible designs of optimal directivity for a given number  $N$  of shells of compact *spherical* multilayer antennas while employing only purely *dielectric* materials. The absence of any metal component makes our designs interesting for space applications. Surprisingly, in spite of limiting ourselves to purely dielectric materials, we have shown that the classical limit for directivity of electrically small resonant antennas can be overcome. We presented (i) a number of superdirective antenna designs and (ii) a stochastic optimization-based recipe to construct new superdirective antennas of a given size and materials. We have also provided a rigorous derivation of the maximum directivity,  $\mathcal{D}$ , for the ultimate superdirective antenna design. Our performance analysis revealed that, as the size of antenna decreases, it is essential to use high refractive index materials to obtain a superdirective antenna radiation pattern. An important property of the proposed designs is their geometrical simplicity: a multilayer sphere excited by a point dipole. It

is anticipated that multiple dipole feeds will be capable of communicating with multiple receiver devices simultaneously using highly directive beams without any mechanical rearrangement. We hope that the results presented here could be applied in the development of subwavelength resonant dielectric antennas for the internet of things and other wireless applications. Our results can be easily adapted for other cases, such as lossy metal materials, which are of significant interest [30] for fluorescence collection and quantum optics, and are the subject of further study. Last but not the least, a duality between electric and magnetic dipole sources enables one to perform an alternative study for a magnetic dipole driven antenna.

#### ACKNOWLEDGMENT

This work was supported by the Ministry of Science and Higher Education of the Russian Federation (Project 075-15-2021-589).

- 
- [1] C. J. Bouwkamp and N. G. de Bruijn, The problem of optimum antenna current distribution, *Philips Res. Rep.* **1**, 135 (1945).
  - [2] L. J. Chu, Physical limitations of omni-directional antennas, *J. Appl. Phys.* **19**, 1163 (1948).
  - [3] H. Riblet, Note on the maximum directivity of an antenna, *Proc. IRE* **36**, 620 (1948).
  - [4] R. Hansen, Fundamental limitations in antennas, *Proc. IEEE* **69**, 170 (1981).
  - [5] R. Harrington, On the gain and beamwidth of directional antennas, *IRE Trans. Antennas Propag.* **6**, 219 (1958).
  - [6] P.-S. Kildal, Fundamental directivity and efficiency limitations of single- and multi-port antennas, in *2nd European Conference on Antennas and Propagation (EuCAP 2007)* (Institution of Engineering and Technology, Edinburgh, UK, 2007), pp. 396–396.
  - [7] P.-S. Kildal, E. Martini, and S. Maci, Degrees of freedom and maximum directivity of antennas: A bound on maximum directivity of nonsuperreactive antennas., *IEEE Antennas Propag. Mag.* **59**, 16 (2017).
  - [8] O. M. Bucci and G. Franceschetti, On the degrees of freedom of scattered fields, *IEEE Trans. Antennas Propag.* **37**, 918 (1989).
  - [9] W. Geyi, Physical limitations of antenna, *IEEE Trans. Antennas Propag.* **51**, 2116 (2003).
  - [10] R. Collin and S. Rothschild, Evaluation of antenna Q, *IEEE Trans. Antennas Propag.* **12**, 23 (1964).
  - [11] A. I. Uzkov, An approach to the problem of optimum directive antenna design, *C. R. (Dokl.) Acad. Sci. URSS* **53**, 35 (1946).
  - [12] M. Pigeon, C. Delaveaud, L. Rudant, and K. Belmaddem, Miniature directive antennas, *Int. J. Microw. Wirel. T.* **6**, 45 (2014).
  - [13] B. Jonsson, S. Shi, L. Wang, F. Ferrero, and L. Lizzi, On methods to determine bounds on the Q-factor for a given directivity, *IEEE Trans. Antennas Propag.* **65**, 5686 (2017).
  - [14] C. Pfeiffer, Fundamental efficiency limits for small metallic antennas, *IEEE Trans. Antennas Propag.* **65**, 1642 (2017).
  - [15] M. Shahpari and D. V. Thiel, Fundamental limitations for antenna radiation efficiency, *IEEE Trans. Antennas Propag.* **66**, 3894 (2018).
  - [16] L. Jelinek, K. Schab, and M. Capek, Radiation efficiency cost of resonance tuning, *IEEE Trans. Antennas Propag.* **66**, 6716 (2018).
  - [17] W. Chen, J. Fu, Q. Wu, and B. Lv, Design principle of cylindrical superdirective antenna, *J. Phys. D* **52**, 495102 (2019).
  - [18] A. Karlsson, On the efficiency and gain of antennas, *PIER* **136**, 479 (2013).
  - [19] M. Majic and E. C. Le Ru, Numerically stable formulation of Mie theory for an emitter close to a sphere, *Appl. Opt.* **59**, 1293 (2020).
  - [20] W. Lin, R. W. Ziolkowski, and J. Huang, Electrically small, low-profile, highly efficient, Huygens dipole rectennas for wirelessly powering internet-of-things devices, *IEEE Trans. Antennas Propag.* **67**, 3670 (2019).
  - [21] R. W. Ziolkowski, Using Huygens Multipole Arrays to Realize Unidirectional Needle-Like Radiation, *Phys. Rev. X* **7**, 031017 (2017).
  - [22] M. Gustafsson and S. Nordebo, Optimal antenna currents for Q, superdirectivity, and radiation patterns using convex optimization, *IEEE Trans. Antennas Propag.* **61**, 1109 (2013).
  - [23] M. Gustafsson and M. Capek, Maximum gain, effective area, and directivity, *IEEE Trans. Antennas Propag.* **67**, 5282 (2019).
  - [24] M. Gustafsson, M. Capek, and K. Schab, Tradeoff between antenna efficiency and Q-factor, *IEEE Trans. Antennas Propag.* **67**, 2482 (2019).
  - [25] See Supplemental Material at <http://link.aps.org/supplemental/10.1103/PhysRevB.104.195406> for details of the analytical and numerical results, which includes Refs. [26,28,30,47–56].
  - [26] A. Moroz, A recursive transfer-matrix solution for a dipole radiating inside and outside a stratified sphere, *Ann. Phys.* **315**, 352 (2005).
  - [27] J. A. Stratton, *Electromagnetics Theory*, International Series in Physics, 1st ed. (McGraw-Hill Book Company, Inc., New York, London, 1941).
  - [28] C. F. Bohren and D. R. Huffman, *Absorption and Scattering of Light by Small Particles* (John Wiley & Sons, New York, 1998).

- [29] H. Chew, P. J. McNulty, and M. Kerker, Model for Raman and fluorescent scattering by molecules embedded in small particles, *Phys. Rev. A* **13**, 396 (1976).
- [30] S. Arslanagić and R. W. Ziolkowski, Highly Subwavelength, Superdirective Cylindrical Nanoantenna, *Phys. Rev. Lett.* **120**, 237401 (2018).
- [31] R. F. Harrington, Effect of antenna size on gain, bandwidth, and efficiency, *J. Res. Natl. Bur. Stand., Sect. D* **64D**, 1 (1960).
- [32] C. C. Lam, P. T. Leung, and K. Young, Explicit asymptotic formulas for the positions, widths, and strengths of resonances in Mie scattering, *J. Opt. Soc. Am. B* **9**, 1585 (1992).
- [33] C. A. Balanis, *Advanced Engineering Electromagnetics*, 2nd ed. (John Wiley & Sons, Inc., New York, 2012).
- [34] R. Gaponenko, I. Rasskazov, A. Moroz, K. Ladutenko, A. Shcherbakov, and P. Belov, Excitation of a homogeneous dielectric sphere by a point electric dipole, [arXiv:2106.06484](https://arxiv.org/abs/2106.06484).
- [35] M. Gastine, L. Courtois, and J. L. Dormann, Electromagnetic resonances of free dielectric spheres, *IEEE Trans. Microwave Theory Tech.* **15**, 694 (1967).
- [36] C. Forestiere, G. Miano, G. Rubinacci, M. Pascale, A. Tamburrino, R. Tricarico, and S. Ventre, Magnetoquasistatic resonances of small dielectric objects, *Phys. Rev. Research* **2**, 013158 (2020).
- [37] List of microwave dielectric resonator materials and their properties, in *Dielectric Materials for Wireless Communication*, edited by M. T. Sebastian (Elsevier, 2008) Appendix 2, pp. 541–652.
- [38] D. G. Baranov, D. A. Zuev, S. I. Lepeshov, O. V. Kotov, A. E. Krasnok, A. B. Evlyukhin, and B. N. Chichkov, All-dielectric nanophotonics: The quest for better materials and fabrication techniques, *Optica* **4**, 814 (2017).
- [39] J. Zhang and A. C. Sanderson, JADE: Adaptive differential evolution with optional external archive, *IEEE Trans. Evolutionary Comput.* **13**, 945 (2009).
- [40] M. Yang, Z. Cai, C. Li, and J. Guan, An improved JADE algorithm for global optimization, in *Proceedings of the 2014 IEEE Congress on Evolutionary Computation, CEC 2014* (IEEE, Piscataway, NJ, 2014), pp. 806–812.
- [41] K. Ladutenko, P.-R. Ovidio, I. Melchakova, I. Yagupov, and P. Belov, Reduction of scattering using thin all-dielectric shells designed by stochastic optimizer, *J. Appl. Phys.* **116**, 184508 (2014).
- [42] IEEE Standards Association, *IEEE Recommended Practice for Near-Field Antenna Measurements* (IEEE, Piscataway, NJ, 2012).
- [43] *Spherical Near-field Antenna Measurements*, edited by J. E. Hansen, IEE Electromagnetic Waves series 26 Peter Peregrinus Ltd. (Peter Peregrinus Ltd., London, United Kingdom, 1988).
- [44] G. Farias, E. Vasconcelos, S. Cesar, and A. Maradudin, Mie scattering by a perfectly conducting sphere with a rough surface, *Physica A* **207**, 315 (1994).
- [45] C. Li, G. W. Kattawar, and P. Yang, Effects of surface roughness on light scattering by small particles, *J. Quant. Spectrosc. Radiat. Transfer* **89**, 123 (2004).
- [46] CST STUDIO SUITE 2019, <https://www.3ds.com/products-services/simulia/products/cst-studio-suite/>.
- [47] A. Edmonds, *Angular Momentum in Quantum Mechanics*, Investigations in physics (Princeton University Press, Princeton, NJ, 1960).
- [48] J. D. Jackson, *Classical Electrodynamics*, 3rd ed. (John Wiley & Sons, Inc., 1999), p. 808.
- [49] L. Tsang, J. A. Kong, and R. T. Shin, *Theory of Microwave Remote Sensing*, Wiley Series in Remote Sensing and Image Processing (Wiley, New York, 1985).
- [50] M. I. Mishchenko, Light scattering by randomly oriented axially symmetric particles, *J. Opt. Soc. Am. A* **8**, 871 (1991).
- [51] H. Chew, Transition rates of atoms near spherical surfaces, *J. Chem. Phys.* **87**, 1355 (1987).
- [52] H. Chew, Radiation and lifetimes of atoms inside dielectric particles, *Phys. Rev. A* **38**, 3410 (1988).
- [53] F. W. Olver, D. W. Lozier, R. F. Boisvert, and C. W. Clark, *The NIST Handbook of Mathematical Functions*, 1st ed. (Cambridge University Press, New York, 2010), <https://www.nist.gov/publications/nist-handbook-mathematical-functions>.
- [54] A. P. Prudnikov, Y. A. Brychkov, and O. I. Marichev, *Integrals and Series. Volume 3: More special functions* (Gordon and Breach Science Publishers, New York, 1990), p. 800.
- [55] M. Abramowitz and I. A. Stegun, *Handbook of Mathematical Functions* (Dover Publications, New York, 1973), p. 1046.
- [56] M. Kerker, D.-S. Wang, and H. Chew, Surface enhanced Raman scattering (SERS) by molecules adsorbed at spherical particles, *Appl. Opt.* **19**, 3373 (1980).